HHS Public Access

Author manuscript

Nat Immunol. Author manuscript; available in PMC 2020 April 21.

Published in final edited form as:

Nat Immunol. 2019 November ; 20(11): 1456–1468. doi:10.1038/s41590-019-0518-7.

RBPJ-dependent Notch signaling initiates the T cell program in a subset of thymus-seeding progenitors

Edward L. Y. Chen[1,2,3], **Patrycja K. Thompson**[1,2,3], **Juan Carlos Zúñiga-Pflücker**[1,2,*]

[1]Sunnybrook Research Institute, Toronto, Ontario, Canada

[2]Department of Immunology, University of Toronto, Toronto, Ontario, Canada

Abstract

T cell specification and commitment requires Notch signaling. Although the requirement for Notch signaling during intrathymic T cell development is known, it is still unclear whether the onset of T cell priming can occur in a pre-thymic niche and whether RBPJ-dependent Notch signaling has a role during this event. Here we established an *Rbpj*-inducible system that allowed the temporal and tissue-specific control of the responsiveness to Notch in all hematopoietic cells. Using this system, we found that Notch signaling was required prior to the early T cell progenitor stage in the thymus. Lymphoid-primed multipotent progenitors in the bone marrow underwent Notch signaling with *Rbpj* induction, which inhibited development towards the myeloid lineage in thymus-seeding progenitors. Thus, our results indicated that the onset of T cell differentiation occurred in a pre-thymic setting, and that Notch played an important role during this event.

T lymphopoiesis in the thymus is contingent on the homing of bone marrow (BM)-derived thymus seeding progenitors (TSPs)[1]. After TSPs enter the thymus, their interaction with thymic stromal cells results in proliferation and commitment to the T cell lineage. A key factor implicated in intrathymic T lineage decisions is Notch signaling[2]. Notch directs T cell specification and commitment[3, 4], and plays a critical role in αβ- vs γδ-lineage bifurcation[5, 6], β-selection[7, 8] and positive selection[9]. However, it is currently unclear whether Notch plays a role prior to thymic entry by initiating T cell differentiation in BM progenitors to generate T lineage competent TSPs. It is currently understood that Notch mediates T lineage commitment by dictating T versus B lineage outcomes[10, 11, 12]. However, whether TSPs first encounter Notch signals and specify to the T cell lineage before or after thymic entry remains unclear. The precise identity of adult TSPs has not been established, but potential candidates include BM-derived lineage $(Lin)^{-}Sca\text{-}1^{+}c\text{-}Kit^{+}Flt\text{-}3^{-}$ hematopoietic stem cells (HSCs), $Lin^{-}Sca\text{-}1^{+}c\text{-}Kit^{+}Flt\text{-}3^{lo}$ multipotent progenitors (MPPs),

*Correspondence should be addressed to J.C.Z-P. (jczp@sri.utoronto.ca). .

Author Contributions

E.L.Y.C. and P.K.T. designed and performed experiments, analyzed the data, and wrote the manuscript. J.C.Z-P. designed experiments, analyzed the data, and wrote the manuscript.

[3]These authors contributed equally to this work

Competing Interests

The authors declare no competing interests. J.C.Z-P. is a founder of Notch Therapeutics.

Lin^{-}Sca-1^{+}c-Kit^{+}Flt-3^{hi} lymphoid-primed multipotent progenitors (LMPPs)[13] and Lin^{-}Sca-1^{lo}c-Kit^{lo}Flt-3^{hi}IL-7Rα^{+} common lymphoid progenitors (CLPs)[14]. Upon entry into the thymus, TSPs are referred to as early T cell progenitors (ETPs) and are found within CD4^{-}CD8^{-} double negative (DN)1a/b cells[15], which are defined as Lin^{-}CD44^{+}CD25^{-}c-Kit^{hi}CD24$^{-/lo}$. ETPs efficiently develop into T cells and have limited B cell potential[15], suggesting that TSPs receive Notch instructive signals in a pre-thymic setting or immediately after thymic entry.

To further elucidate the role of Notch in this regard, here we generated an *Rbpj*-inducible mouse model, which renders all hematopoietic cells unresponsive to Notch signaling and also allows the establishment of their responsiveness in an inducible and temporally-regulated manner. The system reported known Notch-dependent lineage decisions in the hematopoietic system and allowed us to address the temporal and tissue-specific requirements for Notch during T cell development. We found that Notch provided a key pre-thymic signal for the development of ETPs that could generate T cells in the thymus. In addition, we found that BM LMPPs, which represent the likely candidate for adult TSPs[16], underwent Notch signaling in the BM, preventing myeloid lineage skewing within a subset of LMPPs. These findings establish a pre-thymic role for Notch in directing the generation of T lineage competent TSPs.

Results

RBPJ^{ind} mice allow for controlled Notch responsiveness.

Genetic ablations of *Dll1, Dll4, Jag1, Notch1, Notch2* and *Rbpj* result in embryonic or neonatal lethality in mice[17, 18, 19, 20, 21, 22]. To overcome these limitations and to allow the induction and temporal control of Notch responsiveness, and based on the fact that RBPJ interacts with all four Notch receptors23, we generated a mouse model that incorporated conditional deletion of Rbpj and inducible expression of a transgene encoding RBPJ. To conditionally delete Rbpj in hematopoietic cells, RBPJ$^{f/f}$ mice11 were bred to Vav-iCre transgenic (Tg) mice24, generating RBPJ$^{f/f}$Vav-iCre mice (Supplementary Fig. 1a). To induce Notch responsiveness in *Rbpj*-deficient hematopoietic cells, we generated RBPJ-HA Tg mice, in which expression of an HA-tagged RBPJ transgene is under the control of a tetracycline responsive element. Fibroblasts from these mice showed reverse tetracycline-controlled transactivator (rtTA)- and doxycycline (Dox)-dependent expression of the RBPJ-HA transgene (Supplementary Fig. 1b). ROSA26-rtTA mice, in which expression of rtTA is coupled to that of GFP upon Cre-dependent removal of a loxP-stop-loxP cassette within the ROSA26 locus25, were bred to RBPJ-HA Tg mice, generating Tet^{on}RBPJ-HA mice (Supplementary Fig. 1a). RBPJ$^{f/f}$Vav-iCre mice were bred to Tet^{on}RBPJ-HA mice to generate RBPJ$^{f/f}$Vav-iCreTet^{on}RBPJ-HA mice (hereafter RBPJ^{ind}), in which expression of RBPJ-HA in hematopoietic cells can be regulated through presence or absence of Dox *in vivo* (Supplementary Fig. 1a).

Conditional deletion of RBPJ in RBPJ$^{f/f}$Mx-Cre mice leads to arrest of T lymphopoiesis at the DN1 stage, loss of CD4^{+} and CD8^{+} T cells and B cell accumulation in the thymus[11]. Compared to RBPJ-sufficient mice (RBPJ$^{f/+}$Vav-iCreTet^{on}RBPJ-HA; hereafter RBPJ^{Ctr}), the thymus of RBPJ^{ind} mice not treated with Dox (hereafter RBPJ^{ind}-noDox) displayed a block

at the $CD44^{+}CD25^{-}$ DN1 stage and a reduction or near absence of c-$Kit^{hi}CD24^{-/lo}$ DN1a/b cells (Fig. 1a), indicating Notch-RBPJ is required for the generation or maintenance of ETPs[26]. Development of CD4 and CD8 double positive (DP) and single positive (SP) cells, as well as γδ T cells, was abrogated, along with the detection of $B220^{+}CD19^{+}$ B cells and a significant decrease in thymocyte cellularity in the thymus of $RBPJ^{ind}$-noDox mice compared to $RBPJ^{Ctr}$ mice treated with Dox (hereafter $RBPJ^{Ctr}$-Dox mice) (Fig. 1a,b). In $RBPJ^{ind}$ mice treated with Dox for 6 weeks (hereafter $RBPJ^{ind}$-Dox^{6wk}) we detected progression of DN1 cells to $CD44^{+}CD25^{+}$ DN2, $CD44^{-}CD25^{+}$ DN3 and $CD44^{-}CD25^{-}$ DN4 stages, an increase in the percentage of DN1a/b cells (~4-fold), the presence of DPs, SPs and γδ T cells, a decrease in the percentage of B cells (~35-fold), as well as a significant restoration in thymocyte cellularity compared to $RBPJ^{ind}$-noDox mice (Fig. 1a,b). $RBPJ^{ind}$ mice treated with Dox for 3 weeks and analyzed 3 weeks after stopping the Dox treatment (hereafter $RBPJ^{ind}$-Dox^{3wk}-$noDox^{3wk}$) once again displayed a block at the DN1 stage, lacked DN1a/b cells almost entirely and lacked DPs, while $CD4^{+}$ and $CD8^{+}$ SPs and γδ T cells were still present (Fig. 1a). The percentage of thymic B cells was similar to that in $RBPJ^{ind}$-noDox mice, and thymocyte cellularity was decreased compared to $RBPJ^{Ctr}$-Dox and $RBPJ^{ind}$-Dox^{6wk} mice, but higher compared to $RBPJ^{ind}$-noDox mice (Fig. 1a,b).

The organization of cytokeratin 8 $(K8)^{+}\beta5t^{+}$ cortical TECs (cTECs) and $K5^{+}UEA\text{-}1^{+}$ medullary TECs (mTECs)[27] was disrupted in the thymus of $RBPJ^{ind}$-noDox mice compared to $RBPJ^{Ctr}$-Dox mice, while $RBPJ^{ind}$-Dox^{6wk} mice displayed a restoration of thymic architecture (Fig. 2), indicating that T lymphopoiesis induced mature mTEC and cTEC differentiation. $K5^{+}UEA\text{-}1^{+}$ mTECs were detected along with $K5^{+}K8^{+}$ immature cTECs in $RBPJ^{ind}$-Dox^{3wk}-$noDox^{3wk}$ mice, while mature $\beta5t^{+}$ cTECs were absent (Fig. 2), suggesting that maintenance of mature cTECs was dependent on constant supply of T cell progenitors. The thymus of $RBPJ^{ind}$-noDox mice contained $B220^{+}$ B cells that were not confined to the cortico-meduallry junction (CMJ) or the perivascular space (PVS; indicated by Tomato $Lectin^{+}$ endothelial cells), as in $RBPJ^{Ctr}$-Dox mice, but instead were dispersed throughout the thymus parenchyma (Fig. 2). Similar to $RBPJ^{Ctr}$-Dox mice, B cells were restrained to the CMJ and PVS in $RBPJ^{ind}$-Dox^{6wk} mice, while in $RBPJ^{ind}$-Dox^{3wk}-$noDox^{3wk}$ mice, B cells were localized in the expanded cortical niche, similar to $RBPJ^{ind}$-noDox mice (Fig. 2).

Sorted BM $Lin^{-}Sca\text{-}1^{+}c\text{-}Kit^{+}$ cells (LSKs) from $RBPJ^{ind}$-noDox mice cultured on OP9 cells expressing Delta-like-1 (OP9-DL1) for 12 days without Dox did not differentiate into $CD44^{+/-}CD25^{+}$ DN2/DN3 cells, respectively, and became $CD19^{+}$ B cells, in contrast to LSKs from $RBPJ^{Ctr}$ mice (Supplementary Fig. 1c), indicating that controlled Notch responsiveness in $RBPJ^{ind}$ mouse thymus was recapitulated *in vitro*. $RBPJ^{ind}$-noDox LSKs cultured with Dox for 12 days developed into DN2/DN3 cells, while B cells were not detected (Supplementary Fig. 1c), similar to $RBPJ^{Ctr}$ LSKs. Culture of $RBPJ^{ind}$-noDox LSKs with Dox for 8 days followed by removal of Dox for 4 days led to loss of DN2/DN3 development, without the emergence of B cells (Supplementary Fig. 1c), suggesting that initial Notch responsiveness eliminated the B lineage potential. $RBPJ^{ind}$-noDox LSKs cultured on OP9 cells with Dox for 8 days did not give rise to DN2/DN3 cells (Supplementary Fig. 1d), indicating that RBPJ-HA transgene expression did not induce T cell development in the absence of Notch ligands.

CD4$^+$ T cells, CD8$^+$ T cells and γδ T cells were detected in the spleens of RBPJ^{ind}-Dox^{6wk} mice, but not in in RBPJ^{ind}-noDox mice (Supplementary Fig. 2a). These three T cell populations were detected in the spleen of RBPJ^{ind}-Dox^{3wk}-noDox^{3wk} mice (Supplementary Fig. 2a), indicating that Notch was dispensable for the survival of mature T cells. B220$^+$IgM$^+$CD21^{hi}CD23$^-$ marginal zone B (MZB) cells were only detected in RBPJ^{ind}-Dox^{6wk} mice (Supplementary Fig. 2a), confirming that Notch directs the survival of MZB cells[28, 29]. No significant differences in splenocyte cellularity were observed between the mouse groups analyzed (Supplementary Fig. 2b). These results indicated that the RBPJ^{ind} system allowed for temporal regulation of Notch responsiveness *in vivo* and *in vitro*.

Functional ETPs are absent in the RBPJ^{ind}-noDox mouse thymus.

Because the number of DN1a/b cells was markedly reduced in RBPJ^{ind}-noDox mice, we investigated whether maintenance of ETPs required intrathymic Notch signals for their survival or pre-thymic Notch signals for their emergence. To address this, we analyzed the T cell developmental kinetcs in RBPJ^{ind}-Dox mice. CD44$^+$CD25$^+$ DN2 cells were first detected at day 5 post-Dox (Fig. 3a). CD44$^-$CD25$^+$ DN3 cells were detected by day 7, while CD44$^-$CD25$^-$ DN4 cells and CD4$^+$CD8$^+$ DPs appeared robustly by day 11 (Fig. 3a–c), reflecting expected kinetics[2]. Two weeks post-Dox, the distribution of DNs, DPs and SPs in the RBPJ^{ind}-Dox mouse thymus began to resemble steady-state wild-type thymus (Fig. 3a–c).

Because it took 5 days for DN2 cells to appear in the RBPJ^{ind}-Dox mouse thymus, we investigated whether RBPJ^{ind}-noDox mice lacked ETPs. Sorted ETPs and LMPPs, which give rise to TSPs and thus ETPs[16], from RBPJ^{Ctr} mice differentiated into CD44$^+$CD25$^+$ DN2 cells within 1 day and 3 days, respectively, when cultured on OP9-DL4 cells with Dox (Supplementary Fig. 3a), indicating that if ETPs were present in RBPJ^{ind}-noDox mice, then DN2 cells would have appeared within day 1-3 post-Dox, and that the delay in generation of DN2 cells in RBPJ^{ind}-Dox mice suggested an absence of ETPs prior to Dox treatment. ~40% of RBPJ^{ind}-Dox thymocytes were RBPJ-HA$^+$ within 4 hours post-Dox, ~80% by 8 hours, and ~100% by 24 hours (Supplementary Fig. 3b), indicating that the delayed emergence of DN2 cells in the thymi of RBPJ^{ind}-Dox mice was not due to a lag in RBPJ-HA transgene expression.

To investigate whether the delayed appearance of DN2 cells in RBPJ^{ind}-Dox mice was due to disrupted thymic architecture, we performed mixed BM chimeras by injecting equal numbers of CD45.2$^+$(GFP$^-$) wild-type and CD45.2$^+$(GFP$^+$, Supplemental Fig. 1a) RBPJ^{ind}-noDox BM cells into lethally irradiated CD45.1$^+$ wild-type mice. Four weeks after transfer, during which recipient thymic structure was maintained by wild-type donor T cells, recipient mice were Dox-treated and appearance of RBPJ^{ind}-Dox DN2 cells assessed at day 2, 4 and 6 post-Dox initiation. CD45.2$^+$(GFP$^-$) wild-type and CD45.2$^+$(GFP$^+$) RBPJ^{ind}-noDox BM cells, including LSK-Flt-3^{hi} LMPPs, were detected at day 0, prior to Dox treatment (Fig. 4a). Recipient thymi displayed proper segregation of K8$^+$ cTECs and K5$^+$ mTECs at day 0, with CD45.2$^+$(GFP$^-$) wild-type cells showing normal development of DN2, DN3 and DN4 cells, while CD45.2$^+$(GFP$^+$) RBPJ^{ind}-noDox cells were blocked at the DN1 stage (Fig. 4b). Notably, CD45.2$^+$(GFP$^+$) RBPJ^{ind}-Dox DN2 cells were first detected at day 6 post-Dox,

compared to CD45.2^{+}(GFP^{-}) wild-type DN2 cells which were present at all time-points (Fig. 4b). These results indicated that even within a normal thymic structure, RBPJ^{ind}-noDox cells did not appear to give rise to ETPs.

Emergence of functional ETPs depends on Notch signaling.

To further investigate whether Notch signaling initiates T cell differentiation pre-thymically, we examined the T lineage potential of the few Lin^{-}CD44^{+}CD25^{-}c-Kit^{hi}CD24$^{-/lo}$ DN1a/b cells in the thymi of RBPJ^{ind}-noDox mice. We used stringent criteria for the isolation of c-Kit^{hi} DN1a/b cells to exclude c-Kit^{lo} DN1c cells[15] (Supplementary Fig. 4). Sorted DN1a/b cells and BM LSKs from RBPJ^{Ctr} and RBPJ^{ind}-noDox mice were cultured on OP9-DL4 cells in the presence or absence of Dox. RBPJ^{Ctr} LSKs and DN1a/b cells cultured on OP9-DL4 cells gave rise to CD44^{-}CD25^{+} DN3 cells at day 8 and CD4^{+}CD8^{+} DPs at day 14, irrespective of Dox (Fig. 5a,b). RBPJ^{ind}-noDox LSKs on OP9-DL4 cells developed into DN3 cells by day 8 and DPs by day 14 only in the presence of Dox, while RBPJ^{ind}-noDox DN1a/b cells on OP9-DL4 cells did not develop into T lineage cells despite provision of Dox (Fig. 5a,b). These observations indicated that the few thymic DN1a/b cells in RBPJ^{ind}-noDox mice were not T cell progenitors, and that the delayed appearance of DN2 cells following Dox treatment could reflect the requiremet to recruit TSPs that had experienced Notch signals prior to thymic entry. To test this, we sorted DN1a/b cells from RBPJ^{ind} mice treated with Dox for 6 days (hereafter RBPJ^{ind}-Dox^{6d}) and cultured them on OP9-DL4 cells in the presence or absece of Dox. RBPJ^{ind}-Dox^{6d} DN1a/b cells differentiated into DN3 cells at day 8 and DPs at day 14 on OP9-DL4 cells supplemented with Dox, in contrast to RBPJ^{ind}-noDox DN1a/b cells which failed to do so (Fig. 5a,b). RBPJ^{ind}-Dox^{6d} LSKs differentiated into DN3 cells and DPs on OP9-DL4 cells supplemented with Dox, similar to RBPJ^{ind}-noDox LSKs (Fig. 5a,b). These results indicated that thymic appearance of functional ETPs requires Notch signaling pre-thymically.

We also sorted thymic Lin^{-}CD44^{+}CD25^{-}c-Kit^{lo}CD24^{+} DN1c cells and cultured them on OP9-DL4 cells with or without Dox. RBPJ^{Ctr} and RBPJ^{ind}-Dox^{6d} DN1c cells did not develop into DN3 cells (Fig. 5c), consistent with observations that these cells have inefficient T cell potential[15]. RBPJ^{ind}-noDox DN1c cells also did not develop into DN3 cells, albeit CD44^{lo}CD25^{-} B cells were detected in the absence of Dox (Fig. 5c). These experiments excluded the possibility that c-Kit^{lo} TSPs with T cell potential entered the thymus of RBPJ^{ind}-noDox mice in the absence of Notch responsiveness. RBPJ^{Ctr}, RBPJ^{ind}-noDox and RBPJ^{ind}-Dox^{6d} BM LSKs on OP9 cells developed into CD19^{+} B cells at day 14 (Fig. 5d), while RBPJ^{Ctr} and RBPJ^{ind}-Dox^{6d} DN1a/b cells on OP9 did not develop into B cells (Fig. 5d), as expected[15]. RBPJ^{ind}-noDox DN1a/b cells on OP9 also lacked B cell potential (Fig. 5d). These results indicated that the loss of T cell differentiation from RBPJ^{ind}-noDox DN1a/b cells was not due to their divergence to the B cell lineage.

RBPJ^{ind}-noDox DN1a/b cells have myeloid bias.

To determine whether thymic DN1a/b cells from RBPJ^{ind}-noDox mice had dendritic cell (DC) potential[30], sorted BM LSKs and DN1a/b cells from RBPJ^{Ctr}, RBPJ^{ind}-noDox and RBPJ^{ind}-Dox^{6d} mice were cultured on OP9-DL1^{lo} cells with Dox, which support DC differentiation. RBPJ^{Ctr} DN1a/b cells differentiated into CD11c^{+}MHC-II^{+} DCs at day 8

(Supplementary Fig. 5a), consistent with observations that ETPs can generate DCs[30]. RBPJ^{ind}-noDox and RBPJ^{ind}-Dox^{6d} DN1a/b cells had reduced DC potentials compared to RBPJ^{Ctr} DN1a/b cells (~2.5-fold reduction in percentage), while BM LSKs from the different mice developed into DCs equivalently well between each other (Supplementary Fig. 5a). RBPJ^{ind}-noDox and RBPJ^{ind}-Dox^{6d} DN1a/b cells on OP9-DL1^{lo} cells with Dox robustly developed into CD11b^{+}MHC-II^{-} cells by day 8, suggesting a strong myeloid potential, while RBPJ^{Ctr} DN1a/b cells had a limited myeloid potential (Supplementary Fig. 5a). BM LSKs from all mice developed into myeloid cells with similar efficiency (Supplementary Fig. 5a). RBPJ^{ind}-noDox and RBPJ^{ind}-Dox^{6d} DN1a/b cells generated less MHC-II^{lo}B220^{+} plasmacytoid DCs and more MHC-II^{hi}B220^{-}CD11b^{+} myeloid DCs than RBPJ^{Ctr} DN1a/b cells, while BM LSK from all mice gave rise to these subsets with similar efficiency (Supplementary Fig. 5b).

To investigate the transcriptional signature of thymic DN1a/b cells, we performed RNA sequencing analysis on sorted RBPJ^{Ctr}, RBPJ^{ind}-noDox and RBPJ^{ind}-Dox^{6d} DN1a/b cells. Gene expression analysis between samples (≥2-fold different, $P<0.05$) identifyed 66 genes differentially expressed between RBPJ^{Ctr} and RBPJ^{ind}-noDox. RBPJ^{Ctr} DN1a/b cells had high expression of Notch-target genes (*Notch1*, *Hes1*) and T lineage genes (*Tcf7*, *Lck*[31, 32]), while RBPJ^{ind}-noDox DN1a/b cells had high expression of myeloid-specific genes (*Mpo*, *Ctsg*, *Elane*, *Prtn3*[33, 34]), four genes were enriched in RBPJ^{ind}-Dox^{6d} compared to RBPJ^{Ctr} (*Mfsd2b*, *Gata2*, *Apoe*, *Asph*), and nine genes were enriched in RBPJ^{ind}-Dox^{6d} compared to RBPJ^{ind}-noDox (*Notch1*, *Tcf7*) (Fig. 6a,b and Supplementary Tables 1–3). Genes that were highly expressed in RBPJ^{Ctr} DN1a/b cells (*Hes1*, *Tcf7*) or RBPJ^{ind}-noDox DN1a/b cells (*Mpo*, *Elane*) were intermediately expressed in RBPJ^{ind}-Dox^{6d} DN1a/b cells (Fig. 6a), likely due to a mix of Notch-signaled, T cell-competent ETPs and myeloid-specific progenitors in the thymus of these mice. GO analysis[35] on transcripts enriched in RBPJ^{Ctr} or RBPJ^{ind}-noDox DN1a/b cells compared to each other determined that pathways involving genes enriched in RBPJ^{Ctr} included “T cell differentiation” and “αβ T cell differentiation”, while pathways involving genes enriched in RBPJ^{ind}-noDox included “myeloid cell differentiation” and “myeloid cell homeostasis” (Fig. 6c and Supplementary Table 4). These results suggested that the few thymic DN1a/b cells from RBPJ^{ind}-noDox mice lacked T cell potential, but were instead strongly biased toward the myeloid lineage.

BM LMPPs undergo Notch signaling in RBPJ^{ind}-Dox mice.

Because RBPJ^{ind}-noDox mice lacked functional ETPs, we used flow cytometry to examine whether Notch signaling affected BM progenitors with TSP potential, including HSCs, MPPs, LMPPs and CLPs (Supplementary Fig. 6a) in RBPJ^{Ctr} and RBPJ^{ind}-noDox mice. CD62L^{+} LMPPs and Ly6D^{-} CLPs were also analyzed, as these were described to further refine a TSP population[16, 36]. We observed slight but significant decreases in the numbers of MPPs and LMPPs in RBPJ^{ind}-noDox compared to RBPJ^{Ctr}, while the numbers of HSCs and CLPs were not significantly different (Fig. 7a). Additionally, we observed significant decreases in the percentage and number of CD62L^{+} LMPPs in RBPJ^{ind}-noDox compared to RBPJ^{Ctr}, while the percentage and number of Ly6D^{-} CLPs were not significantly different (Fig. 7b).

We next examined which progenitors up-regulated the expression of Notch-target genes upon gaining Notch responsiveness by qPCR analysis. *Hes1* was expressed in RBPJ^{Ctr} HSCs, MPPs, LMPPs and CLPs, while its expression was low in all progenitor subsets from RBPJ^{ind}-noDox BM, with LMPPs and CLPs showing significant decreases in RBPJ^{ind}-noDox compared to RBPJ^{Ctr} (Fig. 7c). *Hes1* expression was not significantly changed in RBPJ^{ind}-Dox^{6d} HSCs, MPPs and CLPs compared to those from RBPJ^{ind}-noDox BM, but its expression was significantly increased in RBPJ^{ind}-Dox^{6d} LMPPs compared to RBPJ^{ind}-noDox LMPPs (Fig. 7c). *Notch1* expression was simiar in all progenitor subsets between RBPJ^{Ctr}, RBPJ^{ind}-noDox and RBPJ^{ind}-Dox^{6d} mice (Fig. 7c). Sorted RBPJ^{ind}-noDox LMPPs differentiated into CD44^{-}CD25^{+} DN3 cells on OP9-DL4 cells with Dox, and did not generate more CD19^{+} B cells on OP9 cells compared to RBPJ^{Ctr} and RBPJ^{ind}-Dox^{6d} LMPPs (Supplementary Fig. 6b). RBPJ^{Ctr} and RBPJ^{ind}-Dox^{6d} LMPPs and CLPs on OP9-DL4 with Dox differentiated into CD44^{+}CD25^{+} DN2 cells with similar kinetics as RBPJ^{ind}-noDox LMPPs and CLPs (day 3) (Supplementary Fig. 6c), suggesting that BM Notch signals do not position LMPPs further ahead the T cell development path. Additionally, limiting dilution analysis of RBPJ^{ind}-noDox CD62L^{+} LMPPs and CLPs on OP9-DL4 cells with Dox showed the same T cell progenitor frequencies (1/1.22-1/1.44) as the RBPJ^{Ctr} counterparts (Supplementary Fig. 7a,b). These results suggested that Notch-unresponsive RBPJ^{ind}-noDox LMPPs undergo Notch signaling in the BM and can effectively initiate the T cell program.

Notch signaling inhibits myeloid potential in BM TSPs.

To investigate the effect of BM Notch signals in TSPs, we performed single-cell RNA sequencing analysis on sorted LSK-Flt-3^{hi} LMPPs from RBPJ^{Ctr} (2614 cells), RBPJ^{ind}-noDox (2729 cells), RBPJ^{ind}-Dox^{3d} (1268 cells) and RBPJ^{ind}-Dox^{6d} (2074 cells) mice. t-SNE analysis of combined cells from all 4 mice identified 8 clusters (cluster 1-8) (Fig. 8a), and gene expression levels were analyzed to identify transcripts enriched in each cluster (≥1.5-fold different, P<0.05) (Supplementary Tables 5–10). Clusters 1 and 2 were not enriched in any particular lineage genes and thus were likely undifferentiated, “stem-like” LMPPs (Fig. 8a). Cluster 3 showed enriched expression of common myeloid progenitor (CMP) genes, e.g., *Cenpa*, *Ccnb2*, *Cdc20* and *Tpx2*[34] (Supplementary Table 5), Cluster 4 showed enriched expression of conventional DC genes, e.g., *H2-Eb1*, *H2-Aa*, *Cd74* and *H2-Ab1*[34] (Supplementary Table 6). Cluster 5 showed enriched expression of genes highly expressed by RBPJ^{Ctr} thymic DN1a/b cells, e.g., *Mn1*, *Emp1*, *Cd33* and *Smad7* (Supplementary Table 7), suggesting these cells possessed T cell progenitor function. Cluster 6 showed enriched expression of plasmacytoid DC genes, e.g., *Isg15*, *Irf7*, *Ifit1* and *Iigp1*[37] (Supplementary Table 8). Cluster 7 showed enriched expression of CLP genes, e.g., *Il7r* and *Rag1*, but also B cell genes, e.g., *Ly6d* and *Ebf1*[38] (Supplementary Table 9). Cluster 8 showed enriched expression of granulocyte-monocyte progenitor (GMP) genes, e.g., *S100a8*, *S100a9*, *Ly6g* and *Lyz2*[34] (Supplementary Table 10).

We next focused on *Sell* (CD62L)$^{+}$ LMPPs and analyzed expression of three important thymus-homing genes: *Selplg* (PSGL-1), *Ccr9* (CCR9) and *Ccr7* (CCR7)[39, 40]. Total LMPPs and LMPPs expressing *Sell*, *Selplg*, *Ccr9* or *Ccr7* from RBPJ^{Ctr} and RBPJ^{ind}-Dox^{6d} mice had significantly higher *Hes1* expression compared to cells from RBPJ^{ind}-noDox mice

(Supplementary Fig. 8a and Supplementary Table 11). *Selplg* expression was not restricted to a particular cluster, but its expression in cluster 5 overlapped with *Ccr9* expression, which was largely restricted to cluster 5 (Fig. 8a). *Ccr7* expression was not restricted to a particular cluster, but its expression in cluster 5 overlapped with *Selplg* and *Ccr9* expression, and only *Sell*$^{+}$ LMPPs from RBPJ^{Ctr}, RBPJ^{ind}-Dox^{3d} and RBPJ^{ind}-Dox^{6d} BM expressed all three genes (Fig. 8a). Of these cells, 100% RBPJ^{Ctr}, 50% RBPJ^{ind}-Dox^{3d} and 75% RBPJ^{ind}-Dox^{6d} cells were located in cluster 5 (Fig. 8b and Supplementary Fig. 8b). Because the proteins encoding these genes contribute to thymus-homing and are expressed by TSPs and ETPs[39, 40, 41], these observations suggested that BM Notch signals in LMPPs induce thymus-seeding capacity. However, *Sell*$^{+}$*Selplg*$^{+}$*Ccr9*$^{+}$ LMPPs were still detected in RBPJ^{ind}-noDox mice (Fig. 8b). Of the 35 *Sell*$^{+}$*Selplg*$^{+}$*Ccr9*$^{+}$ LMPPs in cluster 5, more cells were from from RBPJ^{Ctr} (16) and RBPJ^{ind}-Dox^{6d} (12) mice and each formed a clear cluster, compared to fewer cells from RBPJ^{ind}-noDox mice (5), which did not form a defined cluster (Fig. 8b). Of the overall distribution of *Sell*$^{+}$*Selplg*$^{+}$*Ccr9*$^{+}$ LMPPs, majority of RBPJ^{Ctr} cells located to cluster 5 (16/24), while RBPJ^{ind}-noDox cells showed decreased distribution to cluster 5 (5/14) and increased distribution to cluster 3 (3/24 versus 5/14, respectively), indicating CMP-GMP potential (Fig. 8b). RBPJ^{ind}-Dox^{6d} *Sell*$^{+}$*Selplg*$^{+}$*Ccr9*$^{+}$ LMPPs displayed reduced distribution to cluster 3 compared to RBPJ^{ind}-noDox (1/24) and, more similar to RBPJ^{Ctr}, half of RBPJ^{ind}-Dox^{6d} cells located to cluster 5 (12/24) (Fig. 8b). Distribution of RBPJ^{ind}-noDox, but not RBPJ^{ind}-Dox^{6d}, *Sell*$^{+}$*Selplg*$^{+}$*Ccr9*$^{+}$ LMPPs to cluster 5 significantly deviated (P<0.05) from RBPJ^{Ctr} (Supplementary Table 12).

Among the genes up-regulated (≥1.5-fold, P<0.05) in RBPJ^{ind}-noDox *Sell*$^{+}$*Selplg*$^{+}$*Ccr9*$^{+}$ LMPPs compared to RBPJ^{Ctr} LMPPs (Supplementary Table 13), we detected increased expression of *Egr1*, which was reported to bias MPPs and LMPPs toward the myeloid fate[42, 43], *Klf4* and *Klf2*, which control differentiation of myeloid progenitors to Ly6C^{+} and Ly6C^{-} monocytes, respectively[44, 45], and the AP-1 complex factors, *Fos*, *Fosb*, *Jun* and *Junb*, which control development of specific myeloid lineages[46] (Fig. 8c). Expression of these genes, including *Egr1*, *Klf4* and *Klf2*, was reduced in RBPJ^{ind}-Dox^{6d} *Sell*$^{+}$*Selplg*$^{+}$*Ccr9*$^{+}$ LMPPs compared to RBPJ^{ind}-noDox LMPPs, and as such, the transcriptional profile of RBPJ^{ind}-Dox^{6d} was more similar to RBPJ^{Ctr} (Fig. 8c and Supplementary Tables 14–15). GO analysis[35] on transcripts enriched in RBPJ^{ind}-noDox *Sell*$^{+}$*Selplg*$^{+}$*Ccr9*$^{+}$ LMPPs compred to RBPJ^{Ctr} LMPPs determined that pathways involving these genes included “myeloid leukocyte differentiation” (Supplementary Table 16). Thus, *Sell*$^{+}$*Selplg*$^{+}$*Ccr9*$^{+}$ LMPPs were biased toward the myeloid fate in RBPJ^{ind}-noDox mice, suggesting that BM Notch signaling in TSPs acts to suppress myeloid potential.

Discussion

Here we generated RBPJ^{ind} mice in which hematopoietic cells could be toggled to become responsive to Notch signaling. Using this system, we found that Notch signaling in BM TSPs repressed the myeloid potential of these cells and allowed the up-regulation of a transcriptional program that could coordinate their migration to the thymus. These observations indicated that Notch plays a role in T cell differentiation prior to arrival of TSPs in the thymus.

Mice with *Dll4* conditional deletion have fewer ETPs[26], but evidence for pre-thymic Notch signals in directing T lineage differentiation in TSPs was not documented. Recently, it was shown that BM osteoblasts express DLL4 and appeared to provide Notch signals for the generation of Ly6D^{-} CLPs, which are candidate TSPs[36]. In our study, we could not detect functional ETPs in the thymus of RBPJ^{ind}-noDox mice. Thus, Notch signaling appeared to be required to generate TSPs that give rise to functional ETPs. Notch signaling is thought to be the crucial determinant of T versus B cell decisions, as disruption in Notch signaling led to B cell accumulation in the thymus[10, 11]. However, more recent evidence suggests that inhibition of Notch signaling in ETPs converts them to DCs rather than B cells[30]. In our study, the few thymic DN1a/b cells in RBPJ^{ind}-noDox mice had no T nor B cell potential, but displayed strong myeloid potential and expressed myeloid-specific genes. This finding is consistent with evidence that balance between Notch and PU.1 is important for T cell versus myeloid fate decisions, respectively[47, 48, 49]. Thus, Notch signaling in DN1a/b cells appears to direct T-myeloid, rather than T-B lineage decisions.

Single-cell RNA sequencing of BM LMPPs showed that Notch signals affected the expression of genes that contribute to thymus-homing of TSPs and thus appearance of ETPs in the thymus. This, together with results from the mixed BM chimera mice, suggests that Notch signaling in BM can contribute to the generation of TSPs. Further analysis indicated that RBPJ^{ind}-noDox *Sell*$^{+}$*Selplg*$^{+}$*Ccr9*$^{+}$ LMPPs had higher expression of myeloid differentiation genes compared to RBPJ^{Ctr} and RBPJ^{ind}-Dox^{6d} LMPPS, including *Egr1* and *Klf4*. These genes may be targets of PU.1 and also represent a GMP-specific gene signature[42, 44, 50, 51]. *Egr1* deficiency resulted in more ETPs in the thymus[52], and down-regulation of *Klf4* was required for full T lymphopoiesis to occur in the thymus[53], suggesting that suppression of these factors may be required for the generation of ETPs capable of T cell commitment. Additionally, *Sell*$^{+}$*Selplg*$^{+}$*Ccr9*$^{+}$ LMPPs from RBPJ^{ind}-noDox mice were biased toward the CMP cluster (cluster 3). BM endothelial cells were reported to express DLL4, which was required to prevent myeloid skewing in as early as HSC and MPP stages[54].

However, because RBPJ^{ind}-noDox mice lacked LMPPs with efficient thymus-seeding capacity, we cannot exclude the possibility that thymic entry of LMPP TSPs was completely impaired in the absence of Notch responsiveness. In such a scenario, the myeloid bias of RBPJ^{ind}-noDox DN1a/b cells may be due to presence of CMPs, GMPs or MEPs within the DN1a/b pool[55], and not necessarily conversion of LMPPs to CMPs. This interpretation is still consistent with the idea that lack of BM Notch signals leads to bias of myeloid-committed progenitors within the subset of cells that seed the thymus. Thus, our results indicate that BM Notch signaling inhibits early events of myeloid differentiation in TSPs, and that without these signals, TSPs become fully commited to the myeloid fate upon thymic entry. Altogether, this work revealed an important pre-thymic role for Notch in the generation of T lineage competent TSPs, such that upon thymic entry, ETP functionality is maintained and T cell development can ensue in full.

Methods

Mice.

All mice were bred and maintained in the Comparative Research Facility of the Sunnybrook Research Institute under specific pathogen-free conditions. All animal procedures were approved by the Sunnybrook Research Institute Animal Care Committee and performed in accordance with the committee's ethical standards.

Generation of TetOS-RBPJ-HA transgenic mice.

Mouse RBPJ coding sequence (CDS)[56, 57] lacking a stop codon and carrying a Kozak consensus sequence as well as *Eco*RI and *Sna*BI restriction sites at 5' and 3' end, respectively, was PCR-amplified with Platinum Pfx Polymerase (Invitrogen) from a whole thymus cDNA preparation using the following set of primers: RBPJ-F 5'-ATAGCGAATTCGCCGCAACCATGGCGCCTGTTGTGACA-3' and RBPJ-R 5'-TAATATACGTAGGACACCACGGTTGCTGT-3'. The RBPJ CDS was then cloned into the MIY-II vector using the *Eco*RI and *Sna*BI restriction sites. The hemagglutinin (HA) tag was generated by annealing complementary oligonucleotides (HA-tag F:5'-TATTATACGTAACCAGCTACCCATACGATGTTCCAGATTACGCTTGAGGATCCTGCAT-3' and HA-tag R: 5'-ATGCAGGATCCTCAAGCGTAATCTGGAACATCGTATGGGTAGCTGGTTACGTATAATA-3'), which incorporated a threonine-serine linker at its 5' end as well as *SnaB*I and *Bam*HI sites, and was subsequently annealed into the MIY-RBPJ construct to allow for transgene (Tg) detection and to differentiate it from the endogenously-encoded RBPJ. RBPJ-HA cassette was further subcloned into the pTetOS vector with the use of *Eco*RI and *Bam*HI restriction sites. pTetOS-RBPJ-HA was digested with *Sal*I and the cassette, which included the β-globin intron sequence and a polyA sequence, was ligated into an *Xho*I site of the modified insulator-containing pJC13–1 vector. Insulated TetOS-RBPJ-HA construct was linearized with *Sal*I to remove bacterial DNA elements. Transgenic mice were generated by microinjection of the Tg construct DNA into fertilized eggs obtained from the mating of superovulated C57BL/6J females with C57BL/6J males (The Jackson Laboratory line 000664) at the University of Michigan Transgenic facility, Ann Arbor. Founders and the F1 progeny were screened by PCR for copy number of the Tg by comparing it to the Tg copy standards. Mass of Tg DNA was set as a function of number of base pairs of Tg DNA, the haploid content of a mammalian genome (3×10^9 bp) and amount of tail DNA available. Copy number standards were prepared at 0.01, 0.1, 1, 10, 25 and 50 copies. Primer sequences used were: RBPJ-HA F: 5'-ATGACGGGGTCATTTACTCC-3' and RBPJ-HA R: 5'-CAAGCGTAATCTGGAACATC-3'.

In vitro induction of RBPJ-HA expression in TetOS-RBPJ-HA founders.

Transgenic founder- and F1-derived fibroblasts were prepared by either digesting mouse tails with collagenase IV overnight or by separating two layers of ear tissue and allowing the fibroblasts to adhere to plastic-coated plates. In both cases, cells were grown in Dulbecco's Modified Eagle Medium (DMEM) substituted with 10% fetal bovine serum (FBS), Penicillin-Streptomycin (Pen-Strep) and Hepes-Sodium Pyruvate-Gentamicin mixture. Ten million fibroblasts were transfected with 4 μg of rtTA-containing pTet-DualON vector

(Clontech) using Amaxa nucleofector (Lonza, program U23) and cultured in the presence of 1 μg/ml Dox (Clontech) for 72 hours. Cells were collected and stained for HA in Western blots.

Induction of Notch responsiveness.

To induce transgenic RBPJ-HA expression *in vivo*, 6 to 8 week old RBPJ^{ind} mice were injected with 2 mg/ml Dox (Sigma-Aldrich) intraperitoneally at time 0 and administered 1 mg/ml Dox in drinking water supplemented with 5% Splenda *ad libitum*, with water changed twice a week for the duration of the experiment. Mice not receiving Dox were given drinking water with Splenda alone. RBPJ-HA expression was induced *in vitro* by culturing cells in the presence of 1 μg/ml Dox.

Cell preparation, flow cytometry and cell sorting.

Single-cell suspensions were prepared from mouse BM, thymus and spleen. BM were crushed while thymus and spleen were mashed, then passed through cell strainers while in α-Minimum Essential Medium Eagle (αMEM) supplemented with 20% FBS and 1% Pen-Strep. Erythrocytes were lysed using BD Pharm Lyse™. Single-cell suspensions were stained with antibodies while in Hanks' Balanced Salt Solution (HBSS) supplemented with 1% bovine serum albumin (BSA) and 2mM EDTA. Antibodies were purchased from BD Biosciences, eBiosciences, or BioLegend: CD45.1, CD45.2, MHC-II, CD44, CD25, CD24, CD117, CD4, CD8, CD3, TCRγδ, B220, CD19, IgM, CD21, CD23, NK1.1, CD11b, CD11c, Gr1, Ter119, Sca-1, Flt-3, CD127, CD62L, Ly6D. Anti-HA antibody was purchased from Roche and anti-rat secondary antibody was purchased from Jackson Immunoresearch Laboratories. Intracellular staining for HA was performed using eBiosciences Foxp3/ Transcription Factor Staining Buffer Set. Flow cytometry was performed on LSR II (BD Biosciences) and data analyzed with FlowJo software version 9.9.6. Cell sorting was performed using BD FACSAria IIu.

Immunofluorescence.

Whole thymi were embedded in OCT compound (Tissue-Tek) and snapped frozen in liquid nitrogen. 6 μm tissue slices were obtained using Leica CM3050S and then fixed with 2% paraformaldehyde (Electron Microscopy Sciences) prior to staining. Tissue slices were stained with anti-cytokeratin 5 (Covance), anti-cytokeratin 8 (Troma1), Ulex Europaeus Agglutinin I (UEA-1, Vector Laboratories), anti-β5t (MBL International), anti-B220 (BD Biosciences) or Lycopersicon Esculentum (Tomato) Lectin (Vector Laboratories). Secondary antibodies (anti-rabbit and anti-rat) and streptavidin were purchased from Jackson Immunoresearch Laboratories and BD Biosciences, respectively. Tissue slices were then mounted with Dako fluorescent mounting medium prior to imaging using Zeiss Axiovert 200M.

BM chimera.

1 million whole BM cells from CD45.2^{+}(GFP^{+}) RBPJ^{ind} mice and CD45.2^{+}(GFP^{-}) wild-type mice were mixed and injected into CD45.1^{+} wild=type hosts that were lethally irradiated at 900 rads. After irradiation and injection, hosts were left for 4 weeks to allow

wild-type donor cells to maintain the host thymus. Afterwards, hosts were treated with Dox to assess appearance of DN2 cells from RBPJ^{ind} donor cells.

Cell culture.

BM-derived LSKs, LMPPs and CLPs, and thymus-derived DN1a/b and DN1c cells were purified by flow cytometric cell sorting and cultured on either OP9-DL4, OP9-DL1^{lo} or OP9 cells in αMEM media supplemented with 20% FBS (Gibco) and 1% Pen-Strep, as well as 1 ng/ml of IL-7 and 5 ng/ml of Flt-3L for T-/B- assays, and 100 ng/ml of Flt-3L for myeloid/DC assays (R&D Systems). For T-/B-/myeloid/DC assays from thymic DN1a/b and DN1c cells, ~500 cells were used for each lineage assay for each experiment, with the same numbers used for BM LSK controls. For DN2 differentiation kinetics from ETPs, LMPPs and CLPs, ~2000 cells were used for each day of assessment for each experiment. For single-cell and limiting dilution analysis assays, BM CD62L^{+} LMPPs and CLPs were sorted onto OP9-DL4 cells in 96 well plates at the following doses: 100 cells (12 wells), 30 cells (12 wells), 10 cells (24 wells), 3 cells (24 wells), 1 cell (48 wells), and the T cell progenitor frequency was calculated using ELDA software version 1[58].

Quantitative RT-PCR.

mRNA from sorted BM progenitors were extracted using TRIzol Reagent (ThermoFisher Scientific) and purified. cDNA synthesis and qRT-PCR reaction was performed as one-step using Luna Universal One-Step RT-qPCR Kit, and data was collected using Eppendorf Mastercycler Realplex2. Primers for the following genes were used: *Notch1* (F: 5'-AGATCGACAACCGGCAATGT-3' and R: 5'-CCCACAGCCCACAAAGAAC-3'), *Hes1* (F: 5'-TCCTGACGGCCAATTTGC-3' and R: 5'-GGAAGGTGACACTGCGTTAGG-3'), *β-actin* (F: 5'-GGCTCTTTTCCAGCCTTCCT-3' and R: 5'-GTCTTTACGGATGTCAACGTCACA-3'). Normalized relative expression of *Notch1* and *Hes1* was determined using *β-actin* expression as a housekeeping gene.

RNA sequencing.

Thymic DN1a/b cells were RNA sequenced using NextSeq, and data was analyzed using R software version 3.5.1 with the package edgeR version 1[59]. RNA sequencing products were aligned to the mouse genome (GRCm38) to obtain raw read counts for genes, in which genes not expressed across all samples were removed. Gene expression was normalized between samples to account for variations in library size and sequencing depth. Unsupervised clustering of samples was done, and differential expression analysis of genes was performed after filtering for those that showed at least 2-fold changes between samples, and that were statistically significant[59].

Single-cell RNA sequencing.

BM LMPPs were RNA sequenced at single-cell resolution using 10X Genomics, and data was analyzed using R software version 3.5.1 with the package Seurat version 2.4[60]. Each sample, from a total of 2739 (RBPJ^{Ctr}), 2808 (RBPJ^{ind}-noDox), 1319 (RBPJ^{ind}-Dox^{3d}), 2166 (RBPJ^{ind}-Dox^{6d}) cells, was first filtered to remove cells with low gene counts that arise from aborted sequencing, and gene expression was normalized between cells. Afterwards,

variable expression of genes was determined. All samples were then merged and aligned, and dimensions for t-distributed stochastic neighbor embedding (t-SNE) were calculated to identify unique cell clusters. Cell subsetting based on gene expression was done to identify and analyze TSP populations to determine their cluster location and differential gene expression between samples[60].

Statistical analysis.

The data and error bars are presented as mean ± standard deviation (SD). To determine statistical significance, a two-tailed unpaired t-test was performed using Prism software version 6. Statistical significance was determined as: ns ($P>0.05$), *$P<0.05$, **$P<0.01$, ***$P<0.001$, ****$P<0.0001$. Tests of significance for RNA sequencing and single-cell RNA sequencing data was performed using empirical Bayes moderated t-statistics and Wilcoxon rank sum test, respectively, under R software version 3.5.1, where $P<0.05$ was considered significant.

Reporting Summary.

Further information on research design is available in the “Life Sciences Reporting Summary” linked to this article.

Data Availability

The data that support the findings of this study are available from the corresponding author upon request. Raw and processed RNA sequencing and single-cell RNA sequencing data are available at the Gene Expression Omnibus database under accession number GSE128964.

Supplementary Material

Refer to Web version on PubMed Central for supplementary material.

Acknowledgements

We are grateful to G. Awong and C. McIntosh for their expertise and assistance in flow cytometry and cell sorting, and to C. Lee and L. Wells for their assistance with animal care. We are thankful to R. Dickson and T. McGaha for assistance with the single-cell RNA sequencing analysis, and M. K. Anderson for helpful discussions and critical review of the manuscript. This work was supported by grants from the Canadian Institutes of Health Research (CIHR) MOP-119538 and FND-154332, National Institutes of Health NIH-1P01AI102853-01, and the Krembil Foundation. E.L.Y.C was supported by an Ontario Graduate Scholarship, P.K.T. was supported by a Banting & Best Doctoral Research Award, and J.C.Z-P. is supported by a Canada Research Chair in Developmental Immunology.

References

Methods-only References

1. Takahama Y Journey through the thymus: stromal guides for T-cell development and selection. Nat Rev Immunol 6, 127–135 (2006). [PubMed: 16491137]
2. Petrie HT & Zúñiga-Pflücker JC Zoned out: functional mapping of stromal signaling microenvironments in the thymus. Annu Rev Immunol 25, 649–679 (2007). [PubMed: 17291187]
3. Hozumi K et al. Notch signaling is necessary for GATA3 function in the initiation of T cell development. Eur J Immunol 38, 977–985 (2008). [PubMed: 18383037]

4. Ikawa T, Kawamoto H, Goldrath AW & Murre C E proteins and Notch signaling cooperate to promote T cell lineage specification and commitment. J Exp Med 203, 1329–1342 (2006). [PubMed: 16682500]
5. Ciofani M, Knowles GC, Wiest DL, von Boehmer H & Zuniga-Pflucker JC Stage-specific and differential notch dependency at the alphabeta and gammadelta T lineage bifurcation. Immunity 25, 105–116 (2006). [PubMed: 16814577]
6. Tanigaki K et al. Regulation of alphabeta/gammadelta T cell lineage commitment and peripheral T cell responses by Notch/RBP-J signaling. Immunity 20, 611–622 (2004). [PubMed: 15142529]
7. Ciofani M & Zúñiga-Pflücker JC Notch promotes survival of pre-T cells at the beta-selection checkpoint by regulating cellular metabolism. Nat Immunol 6, 881–888 (2005). [PubMed: 16056227]
8. Maillard I et al. The requirement for Notch signaling at the beta-selection checkpoint in vivo is absolute and independent of the pre-T cell receptor. J Exp Med 203, 2239–2245 (2006). [PubMed: 16966428]
9. Robey E et al. An activated form of Notch influences the choice between CD4 and CD8 T cell lineages. Cell 87, 483–492 (1996). [PubMed: 8898201]
10. Wilson A, MacDonald HR & Radtke F Notch 1-deficient common lymphoid precursors adopt a B cell fate in the thymus. J Exp Med 194, 1003–1012 (2001). [PubMed: 11581321]
11. Han H et al. Inducible gene knockout of transcription factor recombination signal binding protein-J reveals its essential role in T versus B lineage decision. Int Immunol 14, 637–645 (2002). [PubMed: 12039915]
12. Pui JC et al. Notch1 expression in early lymphopoiesis influences B versus T lineage determination. Immunity 11, 299–308. (1999). [PubMed: 10514008]
13. Schwarz BA & Bhandoola A Circulating hematopoietic progenitors with T lineage potential. Nat Immunol 5 (2004).
14. Kondo M, Weissman IL & Akashi K Identification of clonogenic common lymphoid progenitors in mouse bone marrow. Cell 91, 661–672 (1997). [PubMed: 9393859]
15. Porritt HE et al. Heterogeneity among DN1 prothymocytes reveals multiple progenitors with different capacities to generate T cell and non-T cell lineages. Immunity 20, 735–745 (2004). [PubMed: 15189738]
16. Perry SS et al. L-selectin defines a bone marrow analog to the thymic early T-lineage progenitor. Blood 103, 2990–2996 (2004). [PubMed: 15070675]
17. De Bellard ME, Ching W, Gossler A & Bronner-Fraser M Disruption of segmental neural crest migration and ephrin expression in delta-1 null mice. Dev Biol 249, 121–130 (2002). [PubMed: 12217323]
18. Gale NW et al. Haploinsufficiency of delta-like 4 ligand results in embryonic lethality due to major defects in arterial and vascular development. Proc Natl Acad Sci U S A 101, 15949–15954 (2004). [PubMed: 15520367]
19. Xue Y et al. Embryonic lethality and vascular defects in mice lacking the Notch ligand Jagged1. Hum Mol Genet 8, 723–730 (1999). [PubMed: 10196361]
20. Swiatek PJ, Lindsell CE, del Amo FF, Weinmaster G & Gridley T Notch1 is essential for postimplantation development in mice. . Genes Dev 8, 707–719 (1994). [PubMed: 7926761]
21. Tanaka M, Kadokawa Y, Hamada Y & Marunouchi T Notch2 expression negatively correlates with glial differentiation in the postnatal mouse brain. J Neurobiol 41, 524–539 (1999). [PubMed: 10590176]
22. Oka C et al. Disruption of the mouse RBP-J kappa gene results in early embryonic death. Development 121, 3291–3301 (1995). [PubMed: 7588063]
23. Lu FM & Lux SE Constitutively active human Notch1 binds to the transcription factor CBF1 and stimulates transcription through a promoter containing a CBF1-responsive element. Proceedings of the National Academy of Sciences of the United States of America 93, 5663–5667 (1996). [PubMed: 8643633]
24. Stadtfeld M & Graf T Assessing the role of hematopoietic plasticity for endothelial and hepatocyte development by non-invasive lineage tracing. Development 132, 203–213 (2005). [PubMed: 15576407]

25. Belteki G et al. Conditional and inducible transgene expression in mice through the combinatorial use of Cre-mediated recombination and tetracycline induction. Nucleic Acids Res 33, e51 (2005). [PubMed: 15784609]
26. Sambandam A et al. Notch signaling controls the generation and differentiation of early T lineage progenitors. Nat Immunol 6, 663–670 (2005). [PubMed: 15951813]
27. Hamazaki Y Adult thymic epithelial cell (TEC) progenitors and TEC stem cells: Models and mechanisms for TEC development and maintenance. Eur J Immunol 45, 2985–2993 (2015). [PubMed: 26362014]
28. Tanigaki K et al. Notch-RBP-J signaling is involved in cell fate determination of marginal zone B cells. Nat Immunol 3, 443–450 (2002). [PubMed: 11967543]
29. Saito T et al. Notch2 is preferentially expressed in mature B cells and indispensable for marginal zone B lineage development. Immunity 18, 675–685 (2003). [PubMed: 12753744]
30. Feyerabend TB et al. Deletion of Notch1 converts pro-T cells to dendritic cells and promotes thymic B cells by cell-extrinsic and cell-intrinsic mechanisms. Immunity 30, 67–79 (2009). [PubMed: 19110448]
31. De Obaldia ME et al. T cell development requires constraint of the myeloid regulator C/EBP-alpha by the Notch target and transcriptional repressor Hes1. Nat Immunol 14, 1277–1284 (2013). [PubMed: 24185616]
32. Weber BN et al. A critical role for TCF-1 in T-lineage specification and differentiation. Nature 476, 63–68 (2011). [PubMed: 21814277]
33. Yanez A et al. Granulocyte-Monocyte Progenitors and Monocyte-Dendritic Cell Progenitors Independently Produce Functionally Distinct Monocytes. Immunity 47, 890–902 e894 (2017). [PubMed: 29166589]
34. Paul F et al. Transcriptional Heterogeneity and Lineage Commitment in Myeloid Progenitors. Cell 163, 1663–1677 (2015). [PubMed: 26627738]
35. Tripathi S et al. Meta- and Orthogonal Integration of Influenza "OMICs" Data Defines a Role for UBR4 in Virus Budding. Cell host & microbe 18, 723–735 (2015). [PubMed: 26651948]
36. Yu VW et al. Specific bone cells produce DLL4 to generate thymus-seeding progenitors from bone marrow. J Exp Med 212, 759–774 (2015). [PubMed: 25918341]
37. Chen YL et al. A type I IFN-Flt3 ligand axis augments plasmacytoid dendritic cell development from common lymphoid progenitors. The Journal of experimental medicine 210, 2515–2522 (2013). [PubMed: 24145513]
38. Inlay MA et al. Ly6d marks the earliest stage of B-cell specification and identifies the branchpoint between B-cell and T-cell development. Genes & development 23, 2376–2381 (2009). [PubMed: 19833765]
39. Sultana DA, Zhang SL, Todd SP & Bhandoola A Expression of functional P-selectin glycoprotein ligand 1 on hematopoietic progenitors is developmentally regulated. Journal of immunology 188, 4385–4393 (2012).
40. Zlotoff DA et al. CCR7 and CCR9 together recruit hematopoietic progenitors to the adult thymus. Blood 115, 1897–1905 (2010). [PubMed: 19965655]
41. Lai AY & Kondo M Identification of a bone marrow precursor of the earliest thymocytes in adult mouse. Proceedings of the National Academy of Sciences of the United States of America 104, 6311–6316 (2007). [PubMed: 17404232]
42. Spooner CJ, Cheng JX, Pujadas E, Laslo P & Singh H A recurrent network involving the transcription factors PU.1 and Gfi1 orchestrates innate and adaptive immune cell fates. Immunity 31, 576–586 (2009). [PubMed: 19818654]
43. Laslo P et al. Multilineage transcriptional priming and determination of alternate hematopoietic cell fates. Cell 126, 755–766 (2006). [PubMed: 16923394]
44. Alder JK et al. Kruppel-like factor 4 is essential for inflammatory monocyte differentiation in vivo. Journal of immunology 180, 5645–5652 (2008).
45. Mildner A et al. Genomic Characterization of Murine Monocytes Reveals C/EBPbeta Transcription Factor Dependence of Ly6C(−) Cells. Immunity 46, 849–862 e847 (2017). [PubMed: 28514690]
46. Friedman AD C/EBPalpha induces PU.1 and interacts with AP-1 and NF-kappaB to regulate myeloid development. Blood cells, molecules & diseases 39, 340–343 (2007).

47. Franco CB et al. Notch/Delta signaling constrains reengineering of pro-T cells by PU.1. Proceedings of the National Academy of Sciences of the United States of America 103, 11993–11998 (2006). [PubMed: 16880393]

48. Rothenberg EV & Scripture-Adams DD Competition and collaboration: GATA-3, PU.1, and Notch signaling in early T-cell fate determination. Seminars in immunology 20, 236–246 (2008). [PubMed: 18768329]

49. Hosokawa H et al. Transcription Factor PU.1 Represses and Activates Gene Expression in Early T Cells by Redirecting Partner Transcription Factor Binding. Immunity 49, 782 (2018). [PubMed: 30332634]

50. Zhu YP et al. Identification of an Early Unipotent Neutrophil Progenitor with Pro-tumoral Activity in Mouse and Human Bone Marrow. Cell reports 24, 2329–2341 e2328 (2018). [PubMed: 30157427]

51. Drissen R et al. Distinct myeloid progenitor-differentiation pathways identified through single-cell RNA sequencing. Nature immunology 17, 666–676 (2016). [PubMed: 27043410]

52. Schnell FJ, Zoller AL, Patel SR, Williams IR & Kersh GJ Early growth response gene 1 provides negative feedback to inhibit entry of progenitor cells into the thymus. Journal of immunology 176, 4740–4747 (2006).

53. Wen X, Liu H, Xiao G & Liu X Downregulation of the transcription factor KLF4 is required for the lineage commitment of T cells. Cell research 21, 1701–1710 (2011). [PubMed: 22105482]

54. Tikhonova AN et al. The bone marrow microenvironment at single-cell resolution. Nature 569, 222–228 (2019). [PubMed: 30971824]

55. Wolfler A et al. Lineage-instructive function of C/EBPα in multipotent hematopoietic cells and early thymic precursors. Blood (2010).

56. Kawaichi M, Oka C, Reeves R, Kinoshita M & Honjo T Recombination of exogenous interleukin 2 receptor gene flanked by immunoglobulin recombination signal sequences in a pre-B cell line and transgenic mice. J Biol Chem 266, 18387–18394 (1991). [PubMed: 1917962]

57. Matsunami N et al. A protein binding to the J kappa recombination sequence of immunoglobulin genes contains a sequence related to the integrase motif. Nature 342, 934–937 (1989). [PubMed: 2556644]

58. Hu Y & Smyth GK ELDA: extreme limiting dilution analysis for comparing depleted and enriched populations in stem cell and other assays. Journal of immunological methods 347, 70–78 (2009). [PubMed: 19567251]

59. Law CW et al. RNA-seq analysis is easy as 1-2-3 with limma, Glimma and edgeR. F1000Research 5 (2016).

60. Butler A, Hoffman P, Smibert P, Papalexi E & Satija R Integrating single-cell transcriptomic data across different conditions, technologies, and species. Nature biotechnology 36, 411–420 (2018).

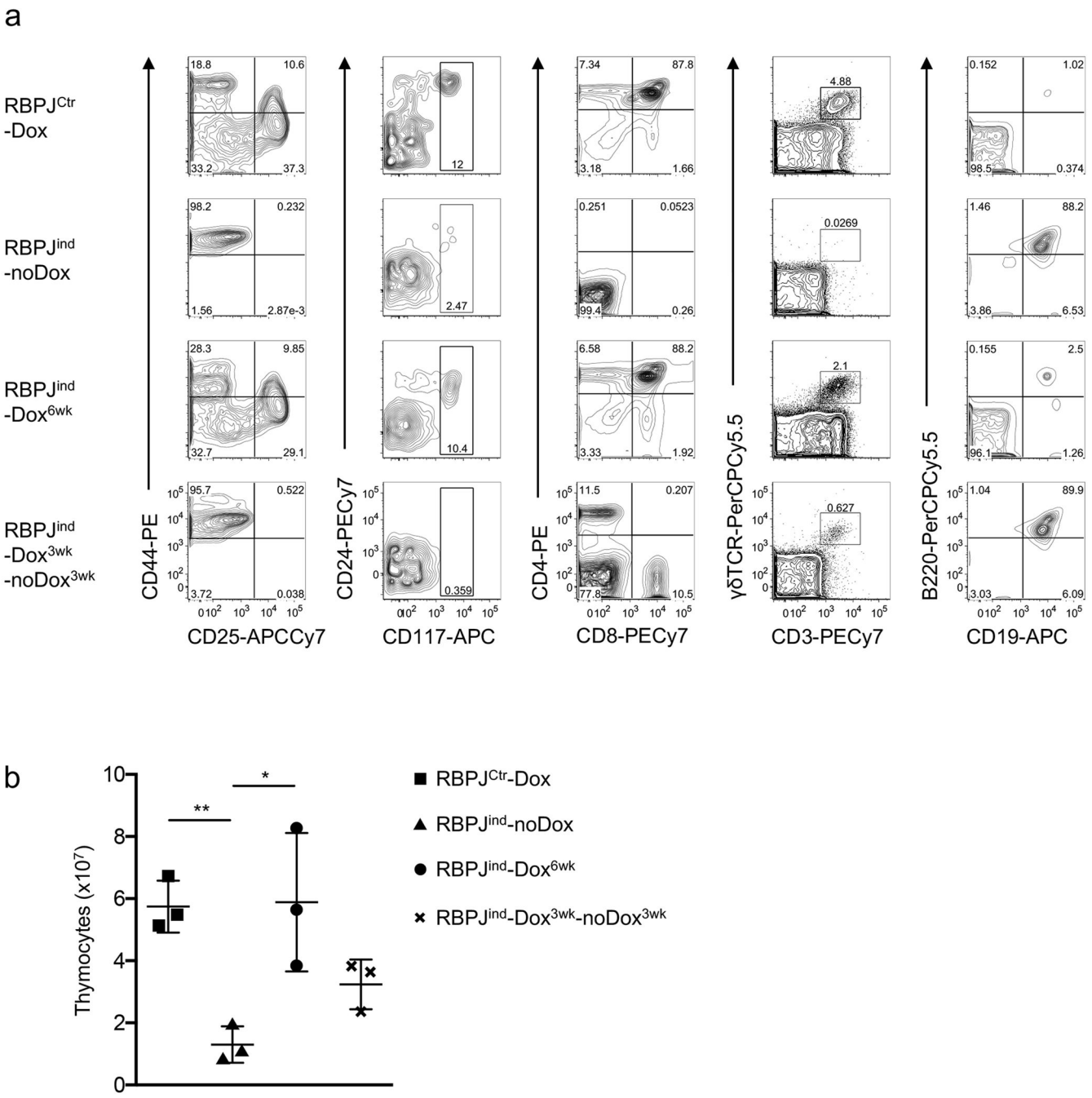

Figure 1. RBPJ^{ind} mice allow for controlled T cell development.

(**a**) Flow cytometry analysis of the thymic phenotype of RBPJ^{Ctr}-Dox, RBPJ^{ind}-noDox, RBPJ^{ind}-Dox^{6wk} and RBPJ^{ind}-Dox^{3wk}-noDox^{3wk} mice. Left to right: analysis of the DN compartment (DN gated), the DN1 compartment (DN1 gated), DPs/SPs, γδ T cells (DN gated) and B cells (DN gated). DN gated: gated on CD4^{-}CD8^{-}. DN1 gated: gated on Lin^{-} (CD8, CD3, NK1.1, B220, CD19, CD11b, CD11c, Gr1, Ter119) CD44^{+}CD25^{-}. Data are representative of three independent experiments (n=3 mice per group). (**b**) Total thymic cellularity of RBPJ^{Ctr}-Dox, RBPJ^{ind}-noDox, RBPJ^{ind}-Dox^{6wk} and RBPJ^{ind}-Dox^{3wk}-

noDox^{3wk} mice showing mean ± standard deviation (n=3 mice per group). *P<0.05, **P<0.01 (two-tailed unpaired t-test).

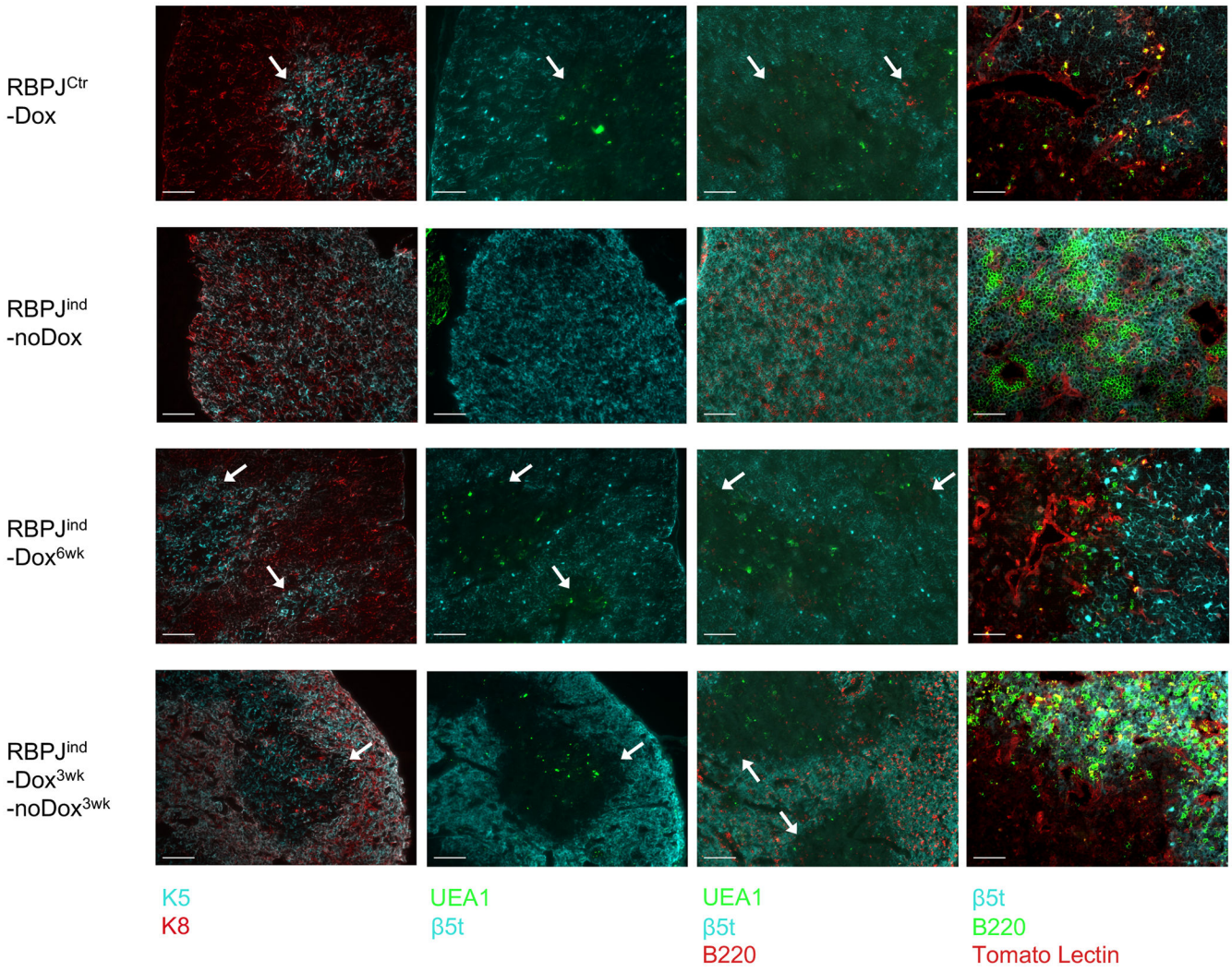

Figure 2. Regulation of T lymphopoiesis in RBPJ^{ind} mice induces thymic architectural changes.

Immunofluorescence analysis of K5, K8, UEA-1 and β5t (left), UEA-1, β5t and B220 (middle; 10x magnification; scale bars denote 100μm) and β5t, B220 and Tomato Lectin (right, 20x magnification; scale bars denote 50μm) in thymic sections from RBPJ^{Ctr}-Dox, RBPJ^{ind}-noDox, RBPJ^{ind}-Dox^{6wk} and RBPJ^{ind}-Dox^{3wk}-noDox^{3wk} mice. The white arrows indicate cortex and medulla boundaries. Data are representative of three independent experiments (n=3 mice per group).

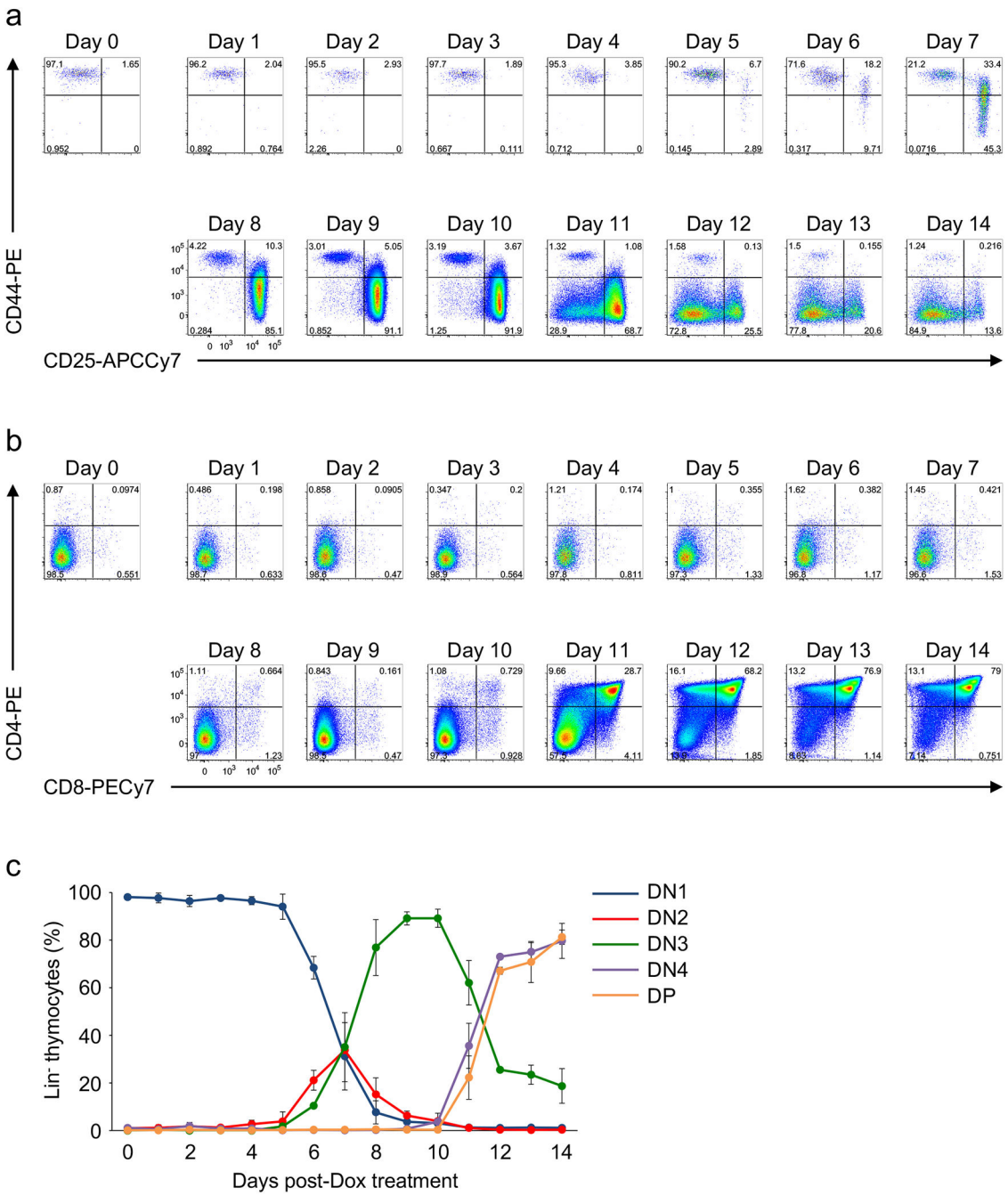

Figure 3. Appearance of DN2 cells in RBPJ^{ind} mouse thymus is delayed upon induction of Notch responsiveness.

(**a-b**) Flow cytometry analysis of the day-by-day progression of (Lin$^-$ pre-gated) DN (a) and DP development (b) in the thymus of RBPJ^{ind}-Dox mice after Dox treatment for 1 to 14 days (as indicated). Data are representative of three independent experiments (n=3 mice per group). (**c**) Percentages of DN subsets and DPs in the thymus of RBPJ^{ind}-Dox mice after Dox treatment for 1 to 14 days (as indicated), showing mean ± standard deviation (n=3 mice per group).

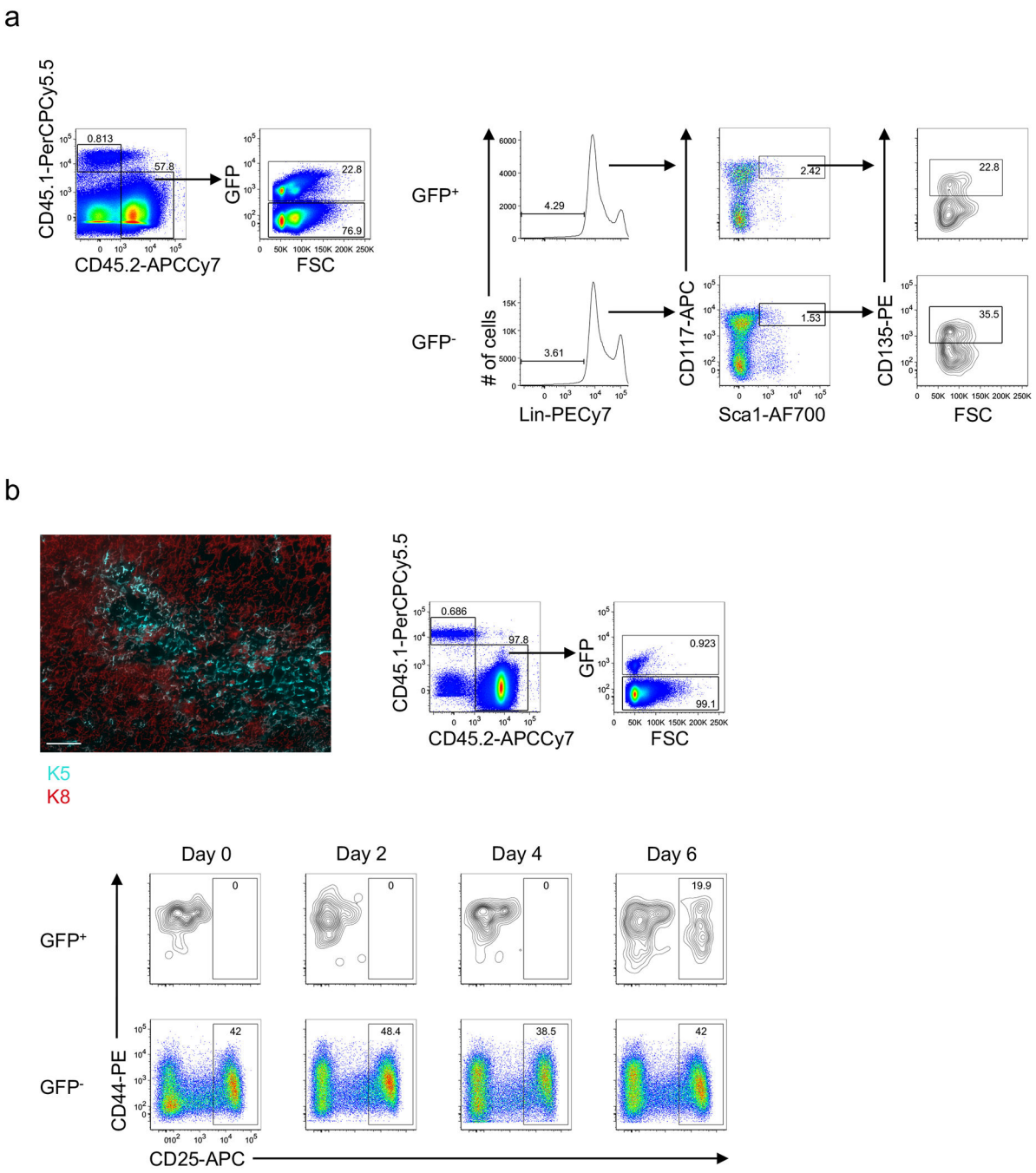

Figure 4. Appearance of RBPJ^{ind} DN2 cells in WT thymus is delayed upon induction of Notch responsiveness.

(**a**) Flow cytometry analysis of BM chimerism of CD45.2^{+}(GFP^{+}) RBPJ^{ind}-noDox donor cells and CD45.2^{+}(GFP^{-}) wild-type (WT) donor cells in lethally irradiated CD45.1^{+} WT mice 4 weeks post-irradiation and BM reconstitution and prior to start of Dox treatment (day 0). (**b**) Immunofluorescence analysis of host thymic architecture at day 0 (10x magnification; scale bars denote 100μm) and flow cytometry analysis of thymic chimerism of RBPJ^{ind}-noDox cells and WT cells on Day 0 (top), and flow cytometry analysis of

kinetics of appearance of $RBPJ^{ind}$-Dox DN2 cells in host mice following 2, 4, and 6 days of Dox treatment (Lin^- pre-gated) (bottom). Data are representative of three independent experiments (n=3 mice per group).

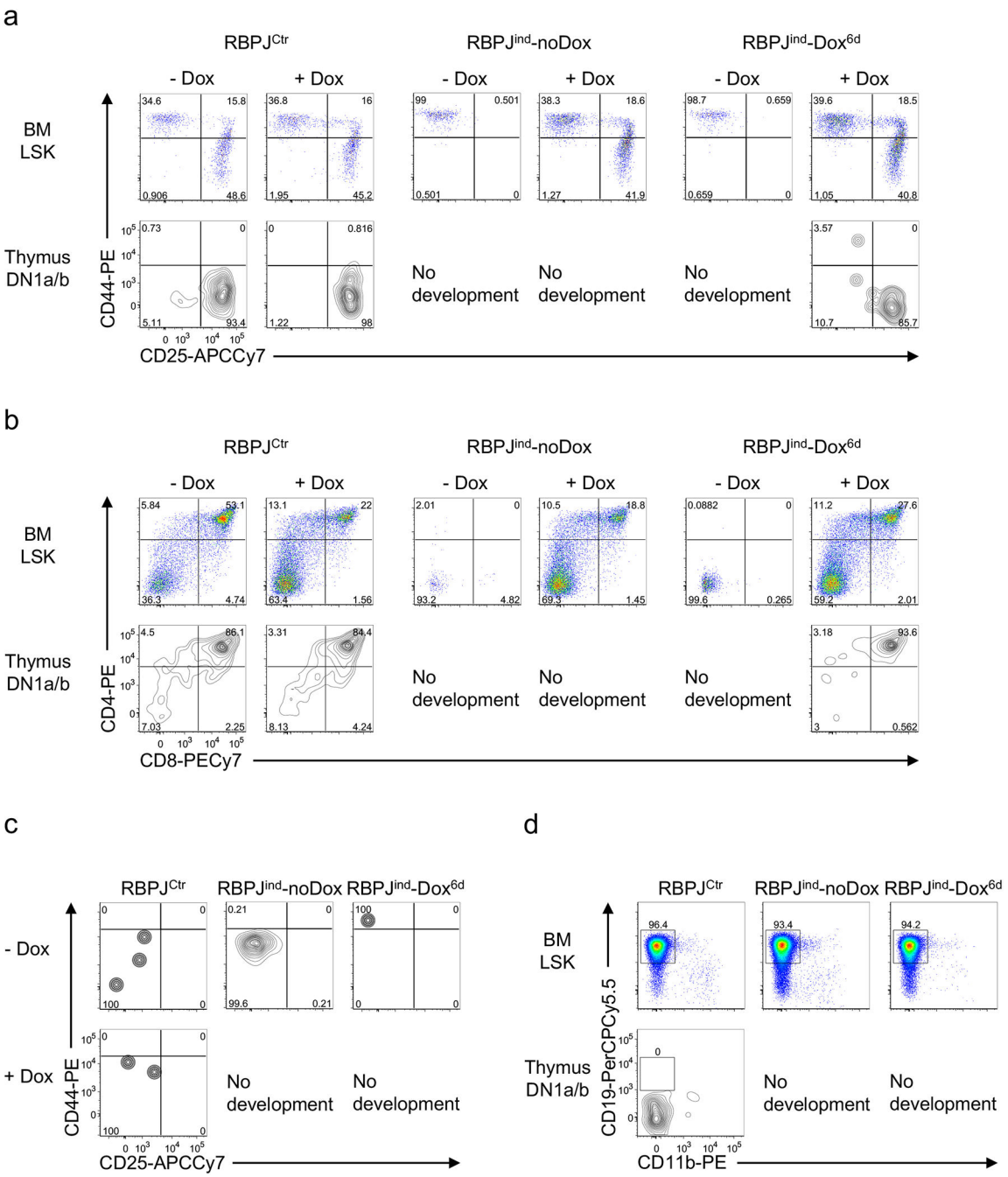

Figure 5. Notch signaling is required for thymic appearance of T lineage competent ETPs.

(**a-b**) Flow cytometry analysis of DN3 and DP development from RBPJ^{Ctr}, RBPJ^{ind}-noDox and RBPJ^{ind}-Dox^{6d} thymic DN1a/b cells and BM LSKs cultured on OP9-DL4 with or without Dox for 8 days (a) and 14 days (b). (**c**) Flow cytometry analysis of DN3 development from RBPJ^{Ctr}, RBPJ^{ind}-noDox and RBPJ^{ind}-Dox^{6d} thymic DN1a/b cells cultured on OP9-DL4 with or without Dox for 8 days. (**d**) Flow cytometry analysis of B cell development from RBPJ^{Ctr}, RBPJ^{ind}-noDox and RBPJ^{ind}-Dox^{6d} thymic DN1a/b cells and BM LSKs cultured on OP9 for 14 days. Data are representative of three independent

experiments (n=2 mice pooled for $RBPJ^{Ctr}$ and n=8 mice pooled for $RBPJ^{ind}$-noDox and $RBPJ^{ind}$-Dox^{6d} for each experiment).

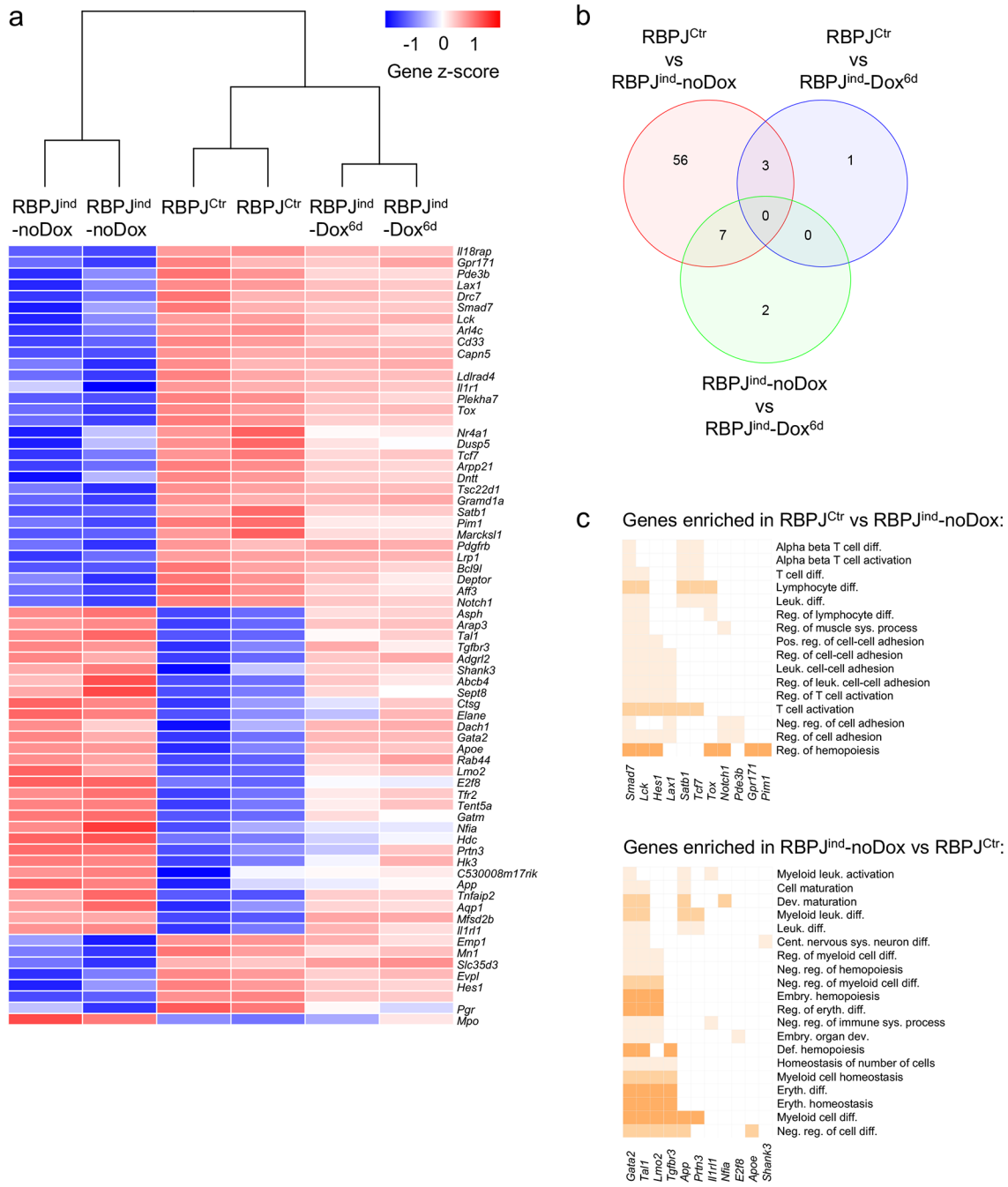

Figure 6. RBPJ^{ind}-noDox thymic DN1a/b cells are myeloid biased.

(**a**) Heatmap analysis of genes enriched in DN1a/b cells sorted from RBPJ^{Ctr}, RBPJ^{ind}-noDox or RBPJ^{ind}-Dox^{6d} mouse thymi. (**b**) Genes differentially expressed between thymic DN1a/b cells of RBPJ^{Ctr}, RBPJ^{ind}-noDox and RBPJ^{ind}-Dox^{6d} mice. For gene expression fold-change values, see Supplementary Tables 1–3. (**c**) GO analysis of biological pathways involving genes enriched in RBPJ^{Ctr} DN1a/b cells compared to RBPJ^{ind}-noDox DN1a/b cells, or genes enriched in RBPJ^{ind}-noDox DN1a/b cells compared to RBPJ^{Ctr} DN1a/b cells. Full names of the biological pathways are described in Supplementary Table 4. Data are

from one independent experiment, where each group was done in duplicates (n=2 mice pooled for $RBPJ^{Ctr}$ and n=8 mice pooled for $RBPJ^{ind}$-noDox and $RBPJ^{ind}$-Dox^{6d} for each replicate).

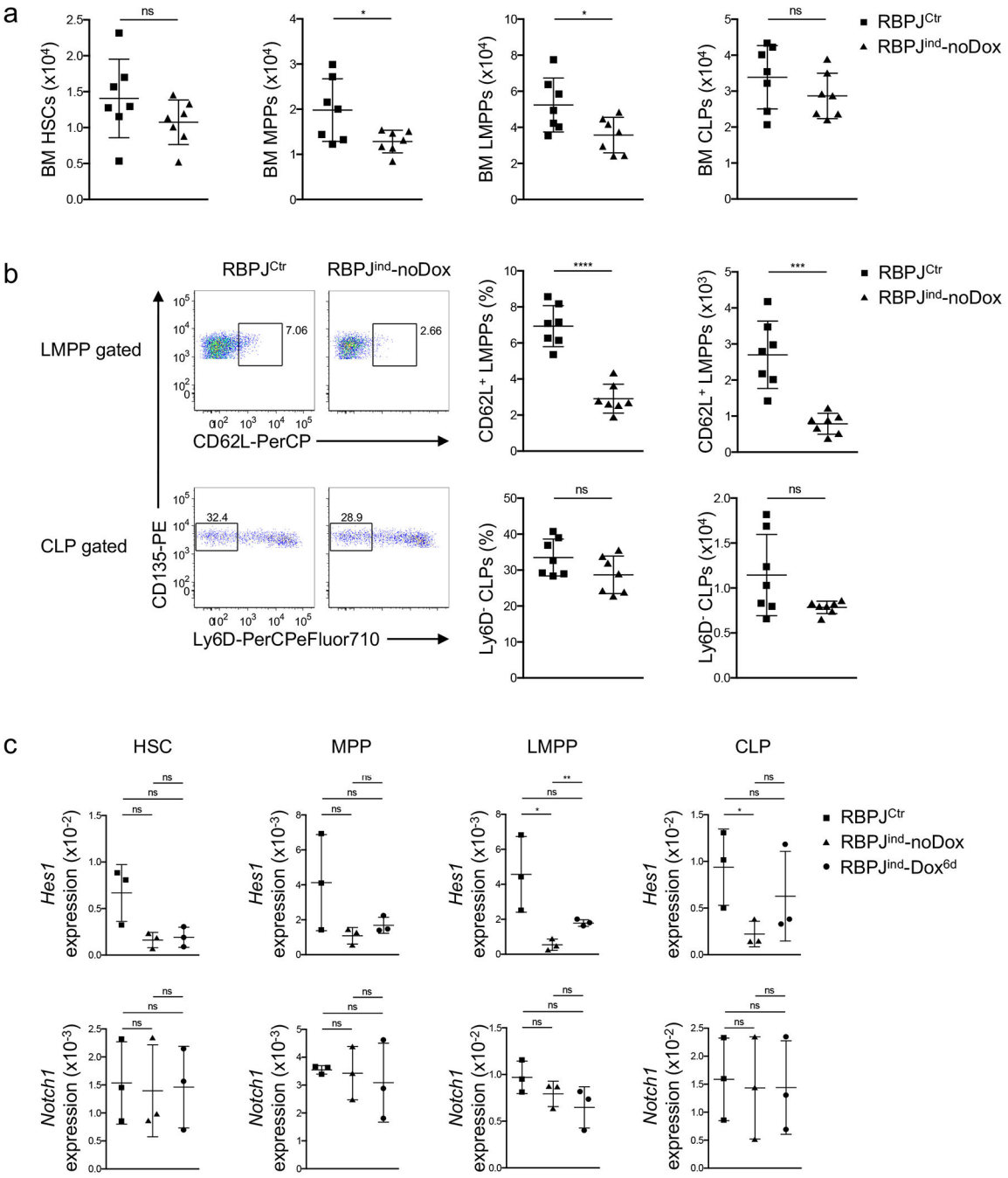

Figure 7. BM LMPPs undergo Notch signaling.

(**a**) Total numbers of BM HSCs, MPPs, LMPPs and CLPs in RBPJ^{Ctr} and RBPJ^{ind}-noDox mice, showing mean ± standard deviation (n=7 mice per group). (**b**) Flow cytometry analysis of BM CD62L^{+} LMPPs and Ly6D^{-} CLPs (left) and percentages and total numbers of BM CD62L^{+} LMPPs and Ly6D^{-} CLPs (right) from RBPJ^{Ctr} and RBPJ^{ind}-noDox mice. Data are representative of four independent experiments (n=7 mice per group; left) and showing mean ± standard deviation (n=7 mice per group; right). (**c**) qPCR analysis of *Hes1* and *Notch1* gene expression by BM HSCs, MPPs, LMPPs and CLPs from RBPJ^{Ctr}, RBPJ^{ind}-noDox and

RBPJ^{ind}-Dox^{6d} mice, showing mean ± standard deviation. Gene expression levels were normalized relative to *β-actin* (n=3 mice pooled for each group for each of the three independent experiments). ns, not significant ($P>0.05$), *$P<0.05$, **$P<0.01$, ***$P<0.001$, ****$P<0.0001$ (two-tailed unpaired t-test).

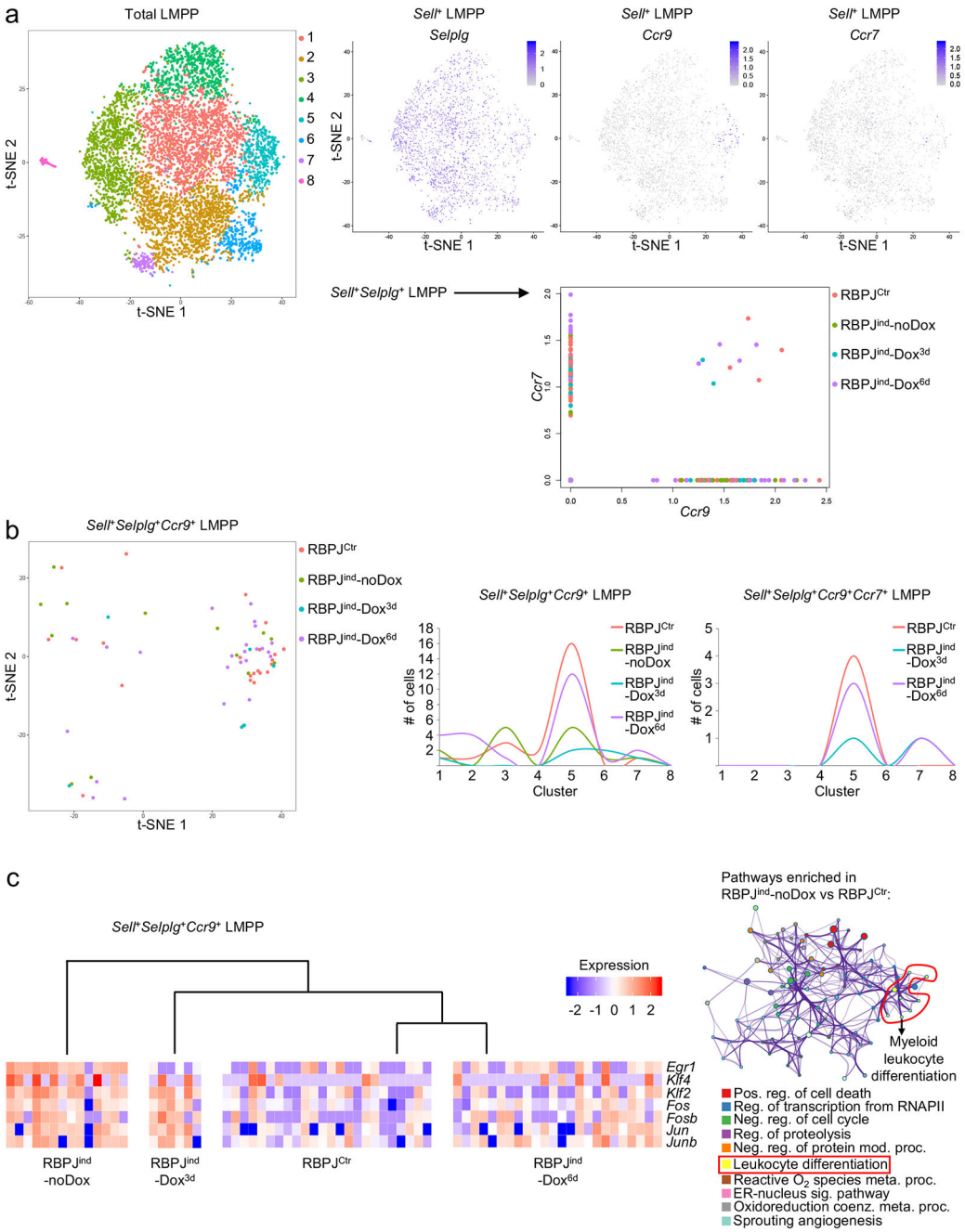

Figure 8. Notch signaling in BM inhibits myeloid skewing in TSPs.

(**a**) t-SNE analysis of 8 clusters from total BM LMPPs (n=8685 cells), analysis of *Selplg*, *Ccr9* and *Ccr7* gene expression in *Sell*$^{+}$ LMPPs (n= 2918 cells), and analysis of *Ccr9* and *Ccr7* gene expression in *Sell*$^{+}$ *Selplg*$^{+}$ LMPPs from RBPJ^{Ctr} mice (n=734 cells), RBPJ^{ind}-noDox mice (n=516 cells), RBPJ^{ind}-Dox^{3d} mice (n=273 cells) and RBPJ^{ind}-Dox^{6d} mice (n=498 cells). For genes enriched in clusters 3-8, see Supplementary Tables 5–10. (**b**) t-SNE analysis of *Sell*$^{+}$ *Selplg*$^{+}$ *Ccr9*$^{+}$ LMPPs from RBPJ^{Ctr}, RBPJ^{ind}-noDox, RBPJ^{ind}-Dox^{3d} and RBPJ^{ind}-Dox^{6d} mice, and overall cluster distribution of *Sell*$^{+}$ *Selplg*$^{+}$ *Ccr9*$^{+}$ LMPPs and *Sell*

$^{+}$*Selplg*$^{+}$*Ccr9*$^{+}$*Ccr7*$^{+}$ LMPPS from RBPJ^{Ctr} mice (n=24 and 4 cells, respectively), RBPJ^{ind}-noDox mice (n=14 cells), RBPJ^{ind}-Dox^{3d} mice (n=6 and 2 cells, respectively) and RBPJ^{ind}-Dox^{6d} mice (n=24 and 4 cells, respectively) (**c**) Heatmap analysis of expression of myeloid differentiation genes in *Sell*$^{+}$*Selplg*$^{+}$*Ccr9*$^{+}$ LMPPs from RBPJ^{Ctr} mice (n=24 cells), RBPJ^{ind}-noDox mice (n=14 cells), RBPJ^{ind}-Dox^{3d} mice (n=6 cells) and RBPJ^{ind}-Dox^{6d} mice (n=24 cells), and GO analysis of the top 10 biological pathways involving genes enriched in RBPJ^{ind}-noDox *Sell*$^{+}$*Selplg*$^{+}$*Ccr9*$^{+}$ LMPPs compared to RBPJ^{Ctr} LMPPs. Full names of the biological pathways are described in Supplementary Table 16. For all genes differentially expressed between RBPJ^{Ctr}, RBPJ^{ind}-noDox and RBPJ^{ind}-Dox^{6d} *Sell*$^{+}$*Selplg*$^{+}$*Ccr9*$^{+}$ LMPPs, see Supplementary Tables 13–15. Names of the biological pathways in the “leukocyte differentiation” cluster and the genes involved are described in Supplementary Table 16. Data are from one independent experiment (n=3 mice pooled for each group).